



OPEN ACCESS

EDITED BY
Stephen Safe,
Texas A&M University, United States

REVIEWED BY
Süleyman Coskun,
Yale University, United States
Ariadna Recasens
Independent Researcher, Melbourne,
VIC, Australia

*CORRESPONDENCE
Michal Yalon
michal@droren.co.il

SPECIALTY SECTION
This article was submitted to
Cancer Molecular Targets
and Therapeutics,
a section of the journal
Frontiers in Oncology

RECEIVED 01 June 2022
ACCEPTED 01 August 2022
PUBLISHED 26 August 2022

CITATION
Eytan K, Versano Z, Oren R,
Jacob-Hirsch J, Leitner M, Harmelin A,
Rechavi G, Toren A, Paglin S and
Yalon M (2022) Pediatric glioblastoma
cells are sensitive to drugs that inhibit
eIF2 α dephosphorylation and its
phosphomimetic S51D variant.
Front. Oncol. 12:959133.
doi: 10.3389/fonc.2022.959133

COPYRIGHT
© 2022 Eytan, Versano, Oren, Jacob-Hirsch,
Leitner, Harmelin, Rechavi, Toren, Paglin and
Yalon. This is an open-access article
distributed under the terms of the [Creative Commons Attribution License \(CC BY\)](https://creativecommons.org/licenses/by/4.0/). The
use, distribution or reproduction in
other forums is permitted, provided
the original author(s) and the
copyright owner(s) are credited and
that the original publication in this
journal is cited, in accordance with
accepted academic practice. No use,
distribution or reproduction is
permitted which does not comply with
these terms.

Pediatric glioblastoma cells are sensitive to drugs that inhibit eIF2 α dephosphorylation and its phosphomimetic S51D variant

Karin Eytan¹, Ziv Versano^{1,2}, Roni Oren³,
Jasmine Jacob-Hirsch^{4,5}, Moshe Leitner¹, Alon Harmelin³,
Gideon Rechavi^{2,4,5}, Amos Toren^{1,2}, Shoshana Paglin¹
and Michal Yalon^{1,6*}

¹Pediatric Hemato-Oncology, Edmond and Lilly Safra Children's Hospital and Cancer Research Center, Sheba Medical Center, Ramat Gan, Israel, ²Sackler School of Medicine, Tel Aviv University, Tel Aviv, Israel, ³Department of Veterinary Resources, The Weizmann Institute of Science, Rehovot, Israel, ⁴Sheba Cancer Research Center (SCRC), Chaim Sheba Medical Center, Ramat Gan, Israel, ⁵Wohl Centre for Translational Medicine, Chaim Sheba Medical Center, Ramat Gan, Israel, ⁶Chaim Sheba Medical Center, Ramat Gan, Israel

We found that pediatric glioblastoma (PED-GBM) cell lines from diffuse intrinsic pontine glioma (DIPG) carrying the H3K27M mutation or from diffuse hemispheric glioma expressing the H3G34R mutation are sensitive to the combination of vorinostat (a histone deacetylase inhibitor) and PARP-1 inhibitors. The combined treatment increased the phosphorylation of eIF2 α (P-eIF2 α) relative to each drug alone and enhanced the decrease in cell survival. To explore the role played by increased P-eIF2 α in modulating PED-GBM survival and response to treatments, we employed brain-penetrating inhibitors of P-eIF2 α dephosphorylation: salubrinal and raphin-1. These drugs increased P-eIF2 α , DNA damage, and cell death, similarly affecting the sensitivity of DIPG cells and derived neurospheres to PARP-1 inhibitors. Interestingly, these drugs also decreased the level of eIF2B ϵ (the catalytic subunit of eIF2B) and increased its phosphorylation, thereby enhancing the effect of increased P-eIF2 α . Transient transfection with the S51D phosphomimetic eIF2 α variant recapitulated the effect of salubrinal and raphin-1 on PED-GBM survival and sensitivity to PARP-1 inhibitors. Importantly, either salubrinal or raphin-1 dramatically increased the sensitivity of DIPG cells to radiation, the main treatment modality of PED-GBM. Finally, PED-GBM was more sensitive than normal human astrocytes to salubrinal, raphin-1, and the treatment combinations described herein. Our results indicate that combinations of histone deacetylase inhibitors and PARP-1 inhibitors should be evaluated for their toxicity and efficacy in PED-GBM patients and point to drugs that increase P-eIF2 α or modulate its downstream effectors as a novel means of treating PED-GBM.

KEYWORDS

pediatric glioblastoma, DIPG, eIF2 α phosphorylation, PARP-1, raphin-1, salubrinal

Introduction

Pediatric glioblastomas (PED-GBM) harboring somatic heterozygous missense H3K27M or H3K34R/V/D mutations are invariably fatal. H3-mutant PED-GBM are distinguished by chromatin modifications, which lead to altered gene expression supporting their specific genetic programs (1–7). H3K27M mutation characterizes the diffuse midline GBM (DMG) tumors located in the pons (DIPG), cerebellum, thalamus, and spine, while H3G34R/V/D-mutant GBM tumors are found in the hemispheric region (8). Consequently, a significant percentage of these tumors are either completely or partially inaccessible for surgical resection. To date, the main treatment modality of PED-GBM is ionizing radiation, which provides only temporary relief. In addition, unlike in adult GBM, the addition of temozolomide in PED-GBM did not show a survival benefit compared to radiation therapy alone, even in tumors with methylated O⁶methylguanine-DNA-methyltransferase (MGMT) promoter (9).

Grasso et al. demonstrated the inhibitory effect of panobinostat, a pan-histone deacetylase inhibitor (HDACi), on the growth of DMG human cell lines in culture and in tumor xenograft models (10), while Chornenkyy et al. showed that niraparib, the brain-penetrating PARP-1 inhibitor (PARPi), decreased survival and enhanced the sensitivity of pediatric high-grade astrocytomas to ionizing radiation both in cell culture and in a tumor xenograft model (11).

Relevant to these studies are the findings that HDACis sensitize breast, ovarian, myeloid leukemia, and prostate cancer cells to treatment with PARPis, regardless of their innate capacity for repairing dsDNA breaks (12–15). We have also previously shown that the combination of vorinostat and veliparib (an HDACi and a PARPi, respectively) enhanced the killing of breast cancer and GBM cell lines, including H3.3G34V-expressing KNS-42 cells (12, 16, 17). To the best of our knowledge, the effect of combining HDACis and PARPis on DMG survival has not been reported to date in either preclinical or clinical trials.

In search of vorinostat downstream effectors that mediate its sensitizing effect on the cellular response to PARPis, we found that vorinostat increased the level of phosphorylation of eIF2 α (P-eIF2 α) in PARPi-treated cells twofold relative to PARPi treatment alone, a phenomenon that in and of itself was sufficient to increase the cellular sensitivity to PARPis (12, 16).

eIF2 α is a subunit of eIF2, which forms a ternary complex with GTP and tRNA^{iMET}. This complex transfers tRNA^{iMET} to the small ribosomal subunit, which, in association with other initiation factors, scans the mRNA until it reaches the start codon, where it is joined by the large ribosomal subunit. Upon recognition of the start codon, GTP is hydrolyzed, and eIF2-GDP is released. Replenishment of eIF2-GTP is executed by eIF2B, a decameric GDP/GTP exchange factor. However, during cellular stress, eIF2 α is phosphorylated, turning eIF2 from a substrate of

eIF2B into its inhibitor, leading to decreased levels of the ternary complex and, with it, to a global attenuation of protein translation (18). In addition to the interaction with P-eIF2 α , the activity of eIF2B is also regulated by the phosphorylation of its catalytic epsilon subunit. Decreased phosphorylation of eIF2Be at S539 increases the GDP/GTP exchange activity of eIF2B and diminishes the inhibitory effect of P-eIF2 α (19, 20). Due to its relatively low cellular level, eIF2B is a rate-limiting factor in the eIF2-GDP/GTP exchange reaction (18). Thus, even relatively small changes in the cellular level of P-eIF2 α , phosphorylated eIF2Be (P-eIF2Be) or eIF2Be may have an impact on the rate of protein translation.

The global attenuation of protein translation goes hand in hand with the increased translation of a subset of mRNAs that mostly code for proteins that modulate the protective response to stress, such as transporters and transcription factors (18, 21). However, to allow for the translation of the newly transcribed mRNAs, the increased P-eIF2 α has to be transient (22). Therefore, a sustained and excessive elevation in P-eIF2 α often leads to cell death (23, 24).

Dephosphorylation of P-eIF2 α is accomplished by protein phosphatase 1 (PP1) in complex with either one of its two regulatory subunits—the constitutive CReP or the stress-induced GADD34—and with G-actin (25–27). The physiological outcome of increased P-eIF2 α has been assessed by employing inhibitors of eIF2 α dephosphorylation (salubrinal and raphin-1) and the non-phosphorylatable (S51A) and phosphomimetic (S51D) eIF2 α variants (16, 28–30). Salubrinal inhibits eIF2 α dephosphorylation by interfering with the interaction of PP1 with its regulatory subunits CReP and GADD34 (28). Its inhibitory effect on isolated holo-phosphatase is reproducible, although milder than that observed within the cells (31). At relatively low concentrations, raphin-1 inhibits the recruitment of P-eIF2 α to the PP1-CReP complex, while at concentrations higher than 10 μ M, it also inhibits the activity of PP1 when in complex with GADD34. Its inhibitory effect on the activity of isolated holo-phosphatase is similar to that observed within cells (32). Both salubrinal and raphin-1 penetrate the blood–brain barrier, but unlike salubrinal, raphin-1 did not adversely affect the long-term memory of the mice (32).

Another compound that can assist in evaluating the role of a moderate increase in cellular P-eIF2 α is ISRIB. Although ISRIB and P-eIF2 α bind to eIF2B at different sites, they do so in a mutually exclusive manner. Therefore, at low P-eIF2 α levels, ISRIB binds to and stabilizes eIF2B, thereby counteracting the effect of increased P-eIF2 α . However, when P-eIF2 α is sustained and excessive, ISRIB fails to bind to and stabilize eIF2B (33).

Modulation of P-eIF2 α also affects the response of cells to anti-neoplastic treatments. While mouse embryonic fibroblasts expressing S51A-eIF2 α are more sensitive to doxorubicin and HDACis than their wild-type counterparts, increased P-eIF2 α mediates IL24-induced death of squamous cell carcinoma, an

effect diminished upon the expression of S51A-eIF2 α (34, 35). Also, ONC201 which demonstrated clinical efficacy toward DMG patients (36) is known to decrease survival and increase P-eIF2 α in colon carcinoma cell lines (37). In addition, we have previously demonstrated that a sustained increase in P-eIF2 α mediates the anti-neoplastic activity of ionizing radiation and vorinostat in a variety of human breast cancer cell lines (16).

In the experiments reported herein, we evaluated the effect of increased P-eIF2 α on PED-GBM survival and response to treatments. Toward that end, we employed raphin-1, salubrinal, and plasmids expressing eIF2 α phosphomimetic variants. The results indicated that increased P-eIF2 α decreases PED-GBM survival and increases PED-GBM's sensitivity to PARPis and ionizing radiation. Increased sensitivity to ionizing radiation is of particular importance in light of the resistance of DIPG to this sole available treatment and the absence of a clinically effective radio enhancer. In addition, to the best of our knowledge, this report shows for the first time the direct effect of increased P-eIF2 α on DNA integrity in cancer cells and the effect of raphin-1 and salubrinal on the ratio of P-eIF2Be to eIF2Be (P-eIF2Be/eIF2Be). The possible mechanisms underlying these two phenomena are discussed herein.

Materials and methods

Cell lines

SU-DIPG-VI-GFP-LUC (SU-DIPG-VI) and SU-DIPG-IV cell lines derived from pediatric DIPG primary tumors expressing H3.3K27M and H3.1K27M, respectively, were a generous gift from Dr. Michelle Monje (Stanford University, Stanford, CA). The KNS-42 cell line, which was derived from a 16-year-old patient glioma and harbors H3.3G34V mutation, was obtained in 2019 from the Japanese Collection of Research Bioresources Cell Bank (Osaka, Japan). Following a short propagation period, these cell lines were frozen, and aliquots were resuscitated and used for 8 weeks. Normal human astrocytes (HAs) were obtained from ScienCell Research Laboratories (Carlsbad, CA). All the cells were routinely tested for the presence of mycoplasma.

Growth conditions

KNS-42 cells were grown in Eagle's minimal essential medium, supplemented with 5% fetal bovine serum (FBS), 1% L-glutamine, penicillin, and streptomycin (Biological Industries, Kibbutz Beit-Haemek, Israel). SU-DIPG-VI and SU-DIPG-IV cells were grown in a tumor stem medium consisting of 50% Neurobasal™-A Medium, 50% DMEM/F-12, 1% HEPES (1 M), 1% sodium pyruvate, 1% non-essential amino acids, 1%

GlutaMAX and 1% antibiotic antimycotic, 2% B-27 (Thermo Fisher Scientific, Waltham, MA), 0.02% heparin (STEMCELL Technologies, Canada), 20 ng/ml EGF and bFGF, and 10 ng/ml PDGF-AA and PDGF-BB (PeproTech Asia, Rehovot, Israel). HA cells were grown in complete astrocyte medium supplemented with 1% penicillin and streptomycin, 2% FBS, and 1% astrocyte growth supplements (all from ScienCell).

Reagents

Vorinostat was obtained from LC Laboratories (Boston, MA), olaparib and niraparib were obtained from MedChemExpress (Monmouth Junction, NJ), salubrinal was obtained from Sigma-Aldrich (Merck KGaA, Darmstadt, Germany), raphin-1 was obtained from Tocris Bioscience (Bristol, UK), and veliparib was obtained from APEXBio (Houston, TX). All the drugs were added from stock solutions in dimethyl sulfoxide (DMSO), and the control cultures received equal amounts of the vehicle. The final concentration of DMSO in the culture medium did not exceed 0.1%. All the other materials were of analytical grade.

Survival assays

SU-DIPG-VI cells were plated in triplicates at a density of 3,500 cells per well in 96-well plates (11,550 cells/cm²). SU-DIPG-IV cells, which grow faster than SU-DIPG-VI cells, were plated in triplicates at a density of 1,000 cells per well in 96-well plates (3,300 cells/cm²). When specified, survival of KNS-42 was determined by plating 500 cells/well in six-well plates (55 cell/cm²) and performing clonogenic assay (16, 38), or by plating 60,000 cells per well in six-well plates (6,600 cells/cm²) for survival assay. At 24 h post-plating, cells from one triplicate were dissociated and counted to determine the cell number at the time of treatment initiation (T₀). Seven to eight days later, the number of surviving cells was determined by counting the trypan blue-excluding cells (T_e). Cell survival was expressed as a percent of control according to the following formula:

$$100 \times \frac{\text{AVG cell \# at } T_e \text{ (treated)} - \text{AVG cell \# at } T_0}{\text{AVG cell \# at } T_e \text{ (control)} - \text{AVG cell \# at } T_0}$$

Cell death was calculated as follows:

$$100 \times \frac{\text{AVG cell \# at } T_0 - \text{AVG cell \# at } T_e}{\text{AVG cell \# at } T_0}$$

The growth rate of HAs was higher than that of SU-DIPG-VI. Therefore, to compare the effects of the various treatments on the number of cell divisions, we plated both cell types at a density of 3,300 cells/cm², which is lower than the regular density of SU-DIPG-VI (11,550 cells/cm²). The cells were

plated in triplicates, and the number of cells at T_0 was determined as described above. The cells were counted 7 days later (T_e), and the percent of cell division relative to control was calculated according to the following formula:

$$100 \times \frac{\log_2(\text{AVG cell \# at } T_e \text{ (treated)})/\text{AVG cell \# at } T_0}{\log_2(\text{AVG cell \# at } T_e \text{ (control)})/\text{AVG cell \# at } T_0}$$

The experimental combination indices (CIs) were obtained by employing the computer program CompuSyn, according to the method used by Chou (39). $CI < 1$ indicated a synergistic interaction, while $CI = 1$ indicated an additive interaction.

SU-DIPG-VI images were captured with the EVOS[®] FL imaging system (Thermo Fisher Scientific, Waltham, MA) with a 10× objective.

Radiation

The cells were irradiated in an X-ray irradiator (Polaris SC-500 series II) 24 h post-plating at a dose rate of 100 cGy/min.

Cell lysis and Western blotting

Unless otherwise noted, treatments were initiated 24 h post-plating for DIPG cells and 48 h post-plating for KNS-42, and incubation was continued for the specified time before the cells were harvested. The cells were washed with ice-cold Dulbecco's phosphate-buffered saline (DPBS) and collected in a buffer containing 150 mM sodium chloride (NaCl), 50 mM Tris (pH 7.5), 2% sodium dodecyl sulfate (SDS), 1.7 mM ethylenediaminetetraacetic acid, 1.5 mM sodium orthovanadate, 100 mM sodium fluoride, 1.5 μg/ml pepstatin, and Roche anti-protease cocktail. Following heating at 95°C and clearing by centrifugation, the protein concentration was determined with a bicinchoninic acid reagent (Bio-Rad, Hercules, CA). Equal loading was verified by measuring the absorbance at 520 nm of Ponceau S extracted with DPBS supplemented with 1.125 M NaCl and 0.6% Tween-20 from individual strips of a twin run (16, 38). Gels were blotted onto nitrocellulose membranes using the Trans-Blot Turbo system (Bio-Rad). Rabbit anti-P-eIF2α, anti-eIF2α, anti-eIF2Be, and anti-HA were obtained from Cell Signaling Technology (Danvers, MA); anti-P-eIF2Be was obtained from Thermo Fisher Scientific (Waltham, MA), anti-CD2 was obtained from Abcam (Cambridge, UK), and HRP-coupled goat anti-rabbit IgG was obtained from Jackson ImmunoResearch Laboratories (West Grove, PA). Blots were exposed to an X-ray film for chemiluminescence following treatment with West Pico ECL reagent (Thermo Fisher Scientific). Values for the integrated light density of autoradiograms were obtained with the ImageJ software and were employed to determine treatment-induced changes in protein levels.

Transfection of cells with plasmid coding for eIF2α variants

WT, S51A, and S51D heIF2α variants in pcDNA3.CD2 expression vectors were obtained from Addgene (Cambridge, MA). WT, S51A, and S51D heIF2α in pcDNA3.1(+)-N-HA were obtained from GenScript USA Inc. (Piscataway, NJ). KNS-42 were plated in six-well plates for clonogenic assay at a density of 55 cells/cm² or for survival assay at a density of 13,200 cells/cm² and transfected 24 h post-plating with eIF2α variants in pcDNA3.CD2 or in pcDNA3.1(+)-N-HA by employing 0.5–1-μg/ml plasmids and jetPEI transfection reagent (Polyplus, New York, NY), according to the manufacturer's instructions.

Alkaline comet assay

SU-DIPG-VI and HAs cells were washed with DPBS, dissociated with diluted TrypLE[™] Express Enzyme (1×) (1:4 in DPBS) (Thermo Fisher, MA), washed with cold DPBS, embedded in agar, and layered over the slides, according to the manufacturer's instructions (Trevigen Inc., Bio-Techne Corporation, Minneapolis, MN). Following incubation with lysis buffer, the cells were further incubated in an alkali solution and then subjected to electrophoresis at 21 V for 18 min. The slides were stained with 1× SYBR Gold and viewed in a fluorescent Nikon Eclipse Ti microscope equipped with a Nikon Intensilight C-HHGFI camera using a 20× objective. The experiments were reproduced three times with DIPG and twice with HAs, and 100 cells were scored for each treatment in each experiment. Cells showing DNA tails, equal to or longer than their radii, were counted as comet-bearing cells. The images for Figure 4 were prepared with PowerPoint software, and the same brightness (+20%) and contrast (-20%) were applied to all panels.

Statistical analysis

The significance of the differences between the surviving fractions of the treatments relative to the untreated control cells and between the combination treatment and each of its components was verified by employing unpaired Student's t-test. $p < 0.05$ in each comparison was considered statistically significant.

Results

The combination of vorinostat and PARPis is deleterious to PED-GBM survival

To test the effect of vorinostat, PARPis, and their combination on PED-GBM survival, we employed three

different specific PARPis: veliparib, olaparib, and niraparib, the most potent of which are olaparib and niraparib (40). Because the H3.3 and H3.1 K27M-mutant DIPG cell lines were reported to respond differently to treatments (41, 42), we included in our experiments both H3.3K27M-SU-DIPG-VI and H3.1K27M-SU-DIPG-IV, along with H3.3G34V-mutant KNS-42. As noted in Figures 1A–F and S1, the combination of vorinostat and PARPis decreased cell survival relative to each drug alone. Under our experimental conditions, the interaction between vorinostat and PARPis was mostly synergistic, or additive at low concentrations of niraparib and vorinostat. The SU-DIPG-VI cells were most sensitive to the combination of vorinostat and niraparib while the SU-DIPG-IV and KNS-42 cells showed similar degrees of sensitivity to the combination of vorinostat with either niraparib or olaparib. In addition, the sensitivity of PED-GBM to the combination of vorinostat and PARPis was higher than that of the HAs (Figures 1J, K). Because astrocytes grow faster in culture than PED-GBM, we had to plate for these experiments a smaller number of DIPG cells than that plated for the experiments shown in Figures 1A, B. This led to an observed increase in the sensitivity of PED-GBM to the drug combinations, relative to that noted in Figures 1A, B.

The enhanced decrease in cell survival was associated with increased P-eIF2 α in the combination-treated cells relative to that triggered by each drug alone (Figures 1G–I). Taken together, these results suggest the possibility that increased P-eIF2 α helps modulate the enhanced response to the combination of vorinostat and PARPis.

Evaluating the role played by increased P-eIF2 α in PED-GBM survival

To explore the effect of increased P-eIF2 α on PED-GBM survival, we employed two inhibitors of P-eIF2 α dephosphorylation: salubrinal and raphin-1 (26, 30). Both drugs led to a dose-dependent increase in P-eIF2 α , which was associated with decreased survival (Figures 2 and 3A–D). Here, PED-GBM also exhibited higher sensitivity to salubrinal or raphin-1 than HAs (Figure 3E). In line with these results, the comet assay showed that incubation with raphin-1 increased the fraction of cells with comet in PED-GBM but failed to do so in HAs (Figure 4). As mentioned earlier, eIF2B is a limiting factor in the process of regenerating the eIF2-GTP-tRNA^{IME_T} ternary complex during protein translation. Therefore, even relatively small changes in its level and phosphorylation are likely to enhance the outcome of increased P-eIF2 α . Unexpectedly, at 15 μ M, both raphin-1 and salubrinal led to a reproducible increase in the ratio of P-eIF2Be/eIF2Be relative to the untreated control cells, which was associated with decreased level of eIF2Be (Figure 3F, S2 and Table S1). This indicates that either the eIF2Be translation decreases or the molecule is being degraded,

but increased kinase activity maintains a higher ratio of P-eIF2Be/eIF2Be. The effect of raphin-1 on the level of eIF2Be was more pronounced than that of salubrinal, which may have been due to the different interactions with the holo-phosphatase, as will be discussed later.

Transient transfection with the phosphomimetic S51D-eIF2 α variant recapitulated the effects of salubrinal and raphin-1 on cell survival. We employed plasmids expressing N-terminal-tagged HA-eIF2 α variants and plasmids expressing the eIF2 α variants and a CD2 reporter (Figures 3G, H and Figure S3). As noted in Figure 3G and S3A, the phosphomimetic eIF2 α variants expressed by either of these plasmids decreased the survival of KNS-42. Transient transfection of KNS-42 with HA-tagged eIF2 α resulted in a time-dependent expression of the different variants. At 12 h post-transfection, similar expression levels of the three variants were detected with anti-HA (Figure 3H). At 24 and 48 h post-transfection, the expressions of HA-eIF2 α and HA-S51A-eIF2 α exceeded that of HA-S51D-eIF2 α , which, in spite of its relatively low cellular level, markedly decreased the level of endogenous eIF2 α (Figure S3C). This effect of the HA-tagged (S51D) variant on the level of eIF2 α was similar to the effects of 15 μ M salubrinal and raphin-1 (Figures 3F, S2).

Salubrinal, raphin-1, and S51D-eIF2 α increase the sensitivity of PED-GBM to PARPis

The combinations of either salubrinal or raphin-1 with olaparib in SU-DIPG-VI and KNS-42 increased P-eIF2 α relative to each drug alone, while the combination of raphin-1 and niraparib in SU-DIPG-VI increased P-eIF2 α relative to niraparib but was similar to that obtained by raphin-1 (Figures 5A–C). Nonetheless, all the combinations enhanced the decrease in cell survival, indicating that treatment with PARPis makes the cells sensitive to increased P-eIF2 α , while treatment with raphin-1 or salubrinal increases the cells' sensitivity to PARPi-specific damage. The combination of raphin-1 and niraparib led to increased DNA damage, as manifested by the fraction of cells with comet induced by this treatment relative to each drug alone. In contrast, raphin-1 failed to increase the fraction of HAs with comet when applied alone or in combination with niraparib (Figure 4). As noted in Figures 5 and S4, the combination of salubrinal or raphin-1 with PARPis enhanced the decrease in cell survival, whether added to single cells 48 h post-plating or to neurospheres 120 h post-plating. In addition, PED-GBM was more sensitive to the combination treatments than HAs (Figures 5G, H). Similar to salubrinal and raphin-1, the phosphomimetic S51D-eIF2 α variant increased the cells' sensitivity to niraparib relative to the non-phosphorylatable S51A or the wild-type variant (Figure 5I).

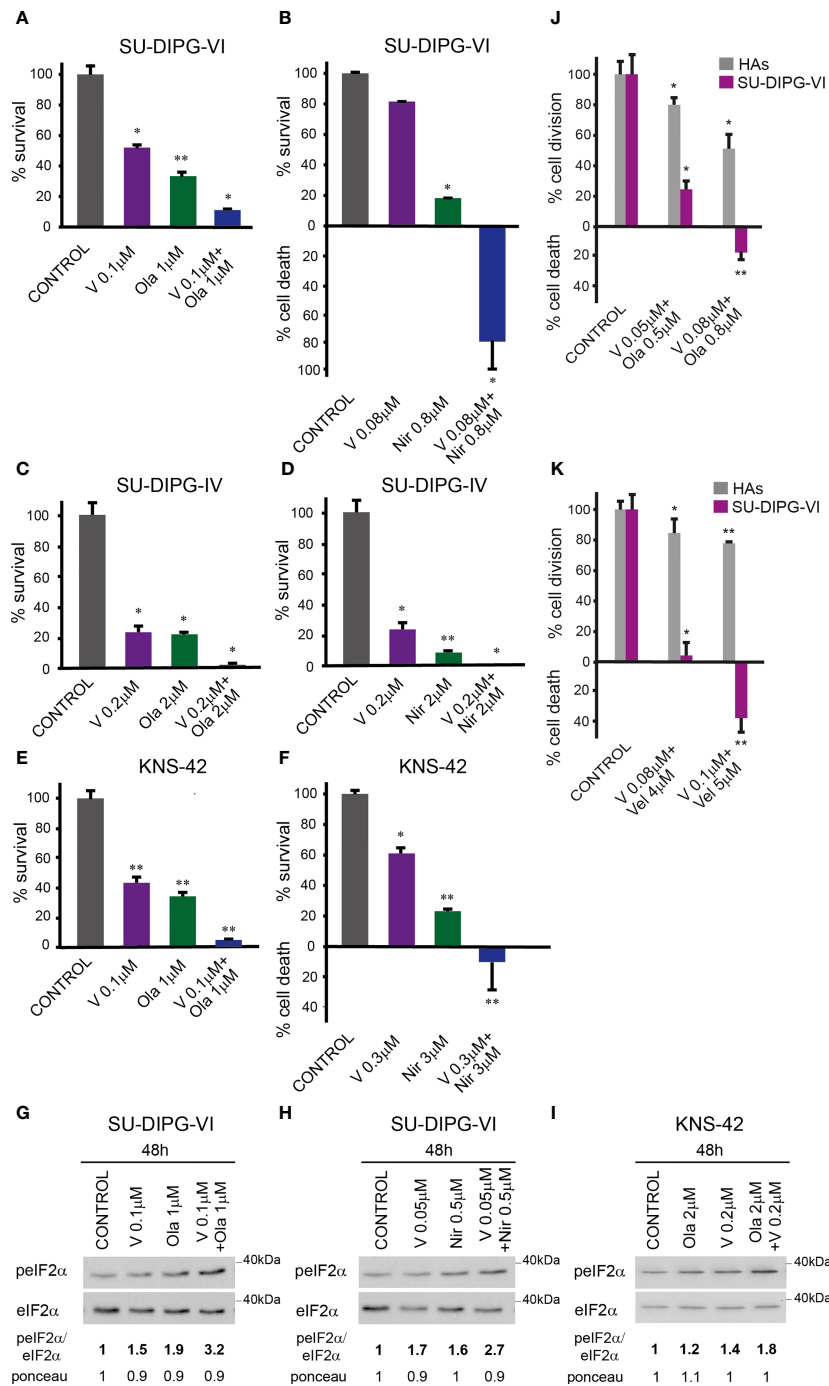


FIGURE 1

Combined treatment of vorinostat and PARPis enhanced the decrease in PED-GBM survival: SU-DIPG-VI cells (A, B) and SU-DIPG-IV cells (C, D) were plated in triplicates at a density of 11,550 or 3,300 cells/cm², respectively. Drugs were added 24 h post-plating. KNS-42 were plated either for clonogenic assay (E) or for survival assay (F) at a density of 55 or 6,600 cells/cm², respectively. Values are mean survival (%) ± S.D relative to control. Differences among all experimental groups, as well as between each experimental group and control, were significant - *p< 0.5, **p< 0.005. (G–I). Cells were processed for Western blot analysis of treatment-induced changes in the ratio of pelf2α/elf2α. Numbers at the bottom of the autoradiograms indicate changes of pelf2α/elf2α and differences in loaded proteins (Ponceau) relative to control. (J, K). SU-DIPG VI and HAs cells were plated in triplicates at the same density (3,300 cells/cm²) and treated with drugs 24 h post-plating. Values are the mean number of cell division or cell death (%) ± S.D relative to control. Differences between treated and untreated experimental groups, as well as between SU-DIPG-VI and HAs, were significant *p< 0.05, **p< 0.005. V—vorinostat, Ola—Olaparib, Vel—veliparib, Nir—niraparib. The experiments were reproduced at least twice with similar results.

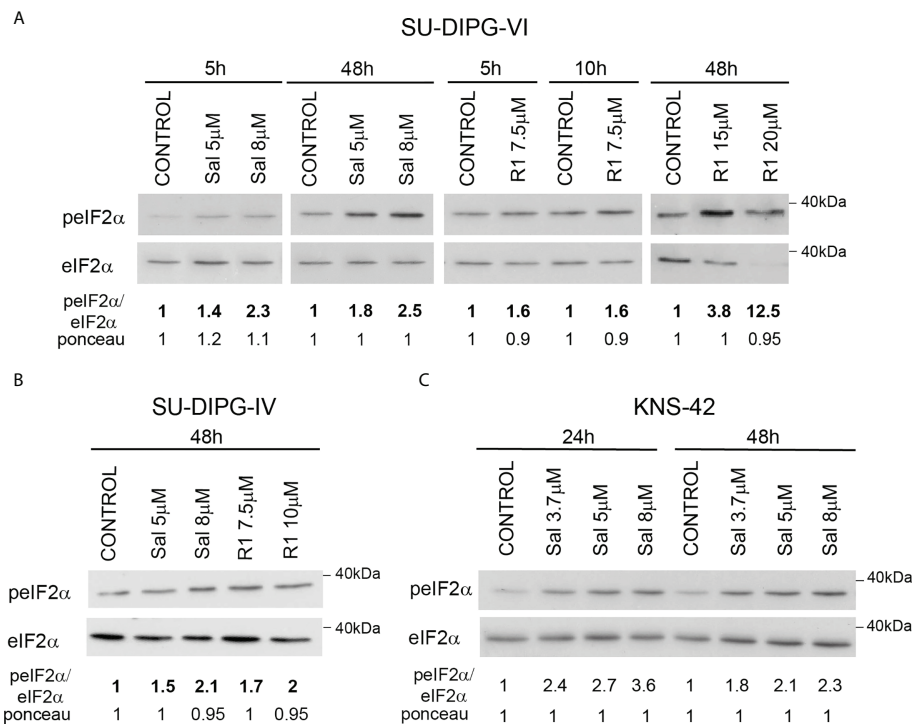


FIGURE 2 Salubrinal and raphin-1 increase P-eIF2 α : (A–C). Cells were processed for Western blot analysis of treatment-induced changes in the ratio of p-eIF2 α /eIF2 α at the indicated time. Numbers at the bottom of the autoradiograms indicate changes of p-eIF2 α /eIF2 α and differences in loaded proteins (Ponceau) relative to control. Sal—salubrinal, R1—raphin-1. The experiments were reproduced at least twice with similar results.

Salubrinal and raphin-1 increase the sensitivity of PED-GBM to ionizing radiation

In light of the transient inhibitory effect of radiation on DMG tumor progression and the absence of a clinically available radio enhancer, we tested the effect of salubrinal and raphin-1 on the sensitivity of SU-DIPG-VI to ionizing radiation. As noted in Figures 6A, B and S5, salubrinal increased the level of P-eIF2 α in the irradiated PED-GBM cells relative to that noted in the cells subjected to irradiation alone and decreased their survival relative to each treatment alone. In addition, the combination of either salubrinal or raphin-1 with 1.5 Gy, which led to cell death in DIPG cells, had only a mild effect on the proliferation of HAs (Figure 6C).

Discussion

PED-GBM responded to the combination of vorinostat and PARPis by enhancing the decrease in cell survival and increasing P-eIF2 α relative to that triggered by each drug alone. Tightly regulated P-eIF2 α is required for maintaining metabolic

demands under basal conditions and in response to stress. Thus, it has been demonstrated that a deficiency in P-eIF2 α signaling due to homozygosity for eIF2 α A/A and excessive phosphorylation resulting from a knockout of CREP interferes with proper embryonic development (30, 33). Therefore, to explore the role played by a sustained increase of P-eIF2 α in PED-GBM survival and response to treatments, we employed inhibitors of P-eIF2 α dephosphorylation and the S51D phosphomimetic variant of eIF2 α .

Both salubrinal and raphin-1 led to a dose-dependent increase of P-eIF2 α and decreased cell survival. Their effects on cell survival were recapitulated by phosphomimetic variants. Interestingly, the phosphomimetic variant and 15 μ M salubrinal and raphin-1 decreased the level of eIF2 α , which, in addition to increasing P-eIF2 α , is bound to further decrease the rate of protein translation. The mechanism underlying the decreased level of eIF2 α , whether by decreasing the level of its mRNA, decreasing translation, or increasing degradation, has yet to be determined.

Our results also demonstrate that 15 μ M raphin-1 or salubrinal decreases the eIF2Be level and increases the ratio of P-eIF2Be/eIF2Be, which is expected to decrease the GDP/GTP exchange activity of eIF2B. Although raphin-1 and salubrinal led to a similar increase in P-eIF2 α , the effect of raphin-1 on the

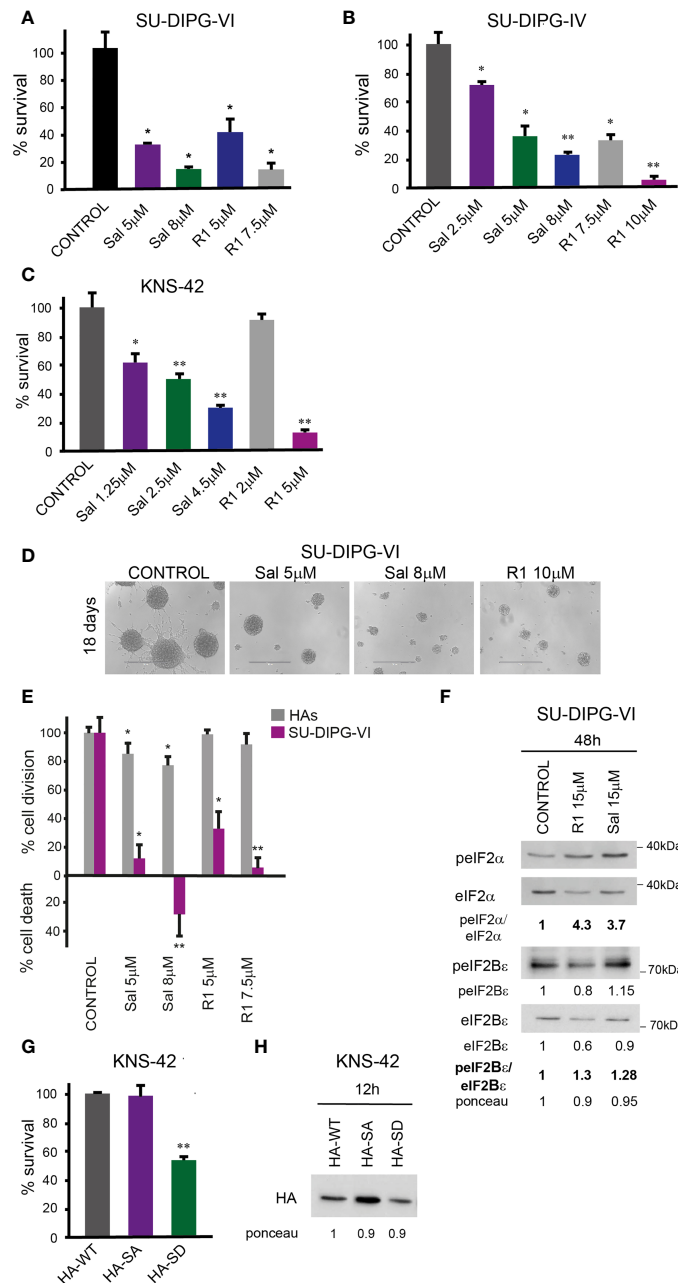


FIGURE 3

Salubrinal and raphin-1, as well as S51D-eIF2α, decreased cell survival and affected the eIF2Bε level and phosphorylation: (A, B) SU-DIPG-VI and SU-DIPG-IV cells were plated in triplicates at a density of 11,550 or 3,300 cells/cm², respectively, and treated 24 h post-plating. (C) KNS-42 cells were plated in triplicates for clonogenic survival assay and treated 24 h post-plating. Values (A–C) are mean survival (%) ± S.D. relative to control. Differences among all experimental groups, as well as between each experimental group and control, were significant—*p < 0.05, **p < 0.005. (D) A representative image of SU-DIPG-VI neurospheres 18 days post-treatment with salubrinal and raphin-1. Bar, 400 μm. (E) SU-DIPG-VI and HAs cells were plated in triplicates at the same density (3,300 cells/cm²) and treated 24 h post-plating. Values are mean number of cell division or cell death (%) ± S.D. relative to control. Differences between treated and untreated experimental groups, as well as between SU-DIPG-VI and HAs, were significant—*p < 0.05, **p < 0.005. (F) SU-DIPG-VI cells were processed for Western blot analysis of treatment-induced changes in the ratios of peIF2α/eIF2α and peIF2Bε/eIF2Bε and in the cellular level of eIF2Bε. Numbers at the bottom of the autoradiograms indicate changes of peIF2α/eIF2α, peIF2Bε/eIF2Bε, and eIF2Bε and differences in loaded proteins (Ponceau) relative to control. (G) KNS-42 cells were plated in duplicates at a density of 13,200 cells/cm² and transiently transfected with 1 μg/ml of plasmids expressing HA-eIF2α (HA-WT) or HA-S51A-eIF2α (HA-SA) or with HA-S51D-eIF2α (HA-SD) 24 h post-plating. Values are mean survival (%) ± S.D. relative to control. Differences between survival of HA-SD to the HA-WT and HA-SA were significant—**p < 0.005. (H) Cells were transiently transfected as described in G and 12 h later processed for Western blot analysis of HA-tag expression. Numbers at the bottom of the autoradiograms indicate differences in loaded proteins (Ponceau) relative to HA-WT. Sal—salubrinal, R1—raphin-1. The experiments were reproduced at least twice with similar results.

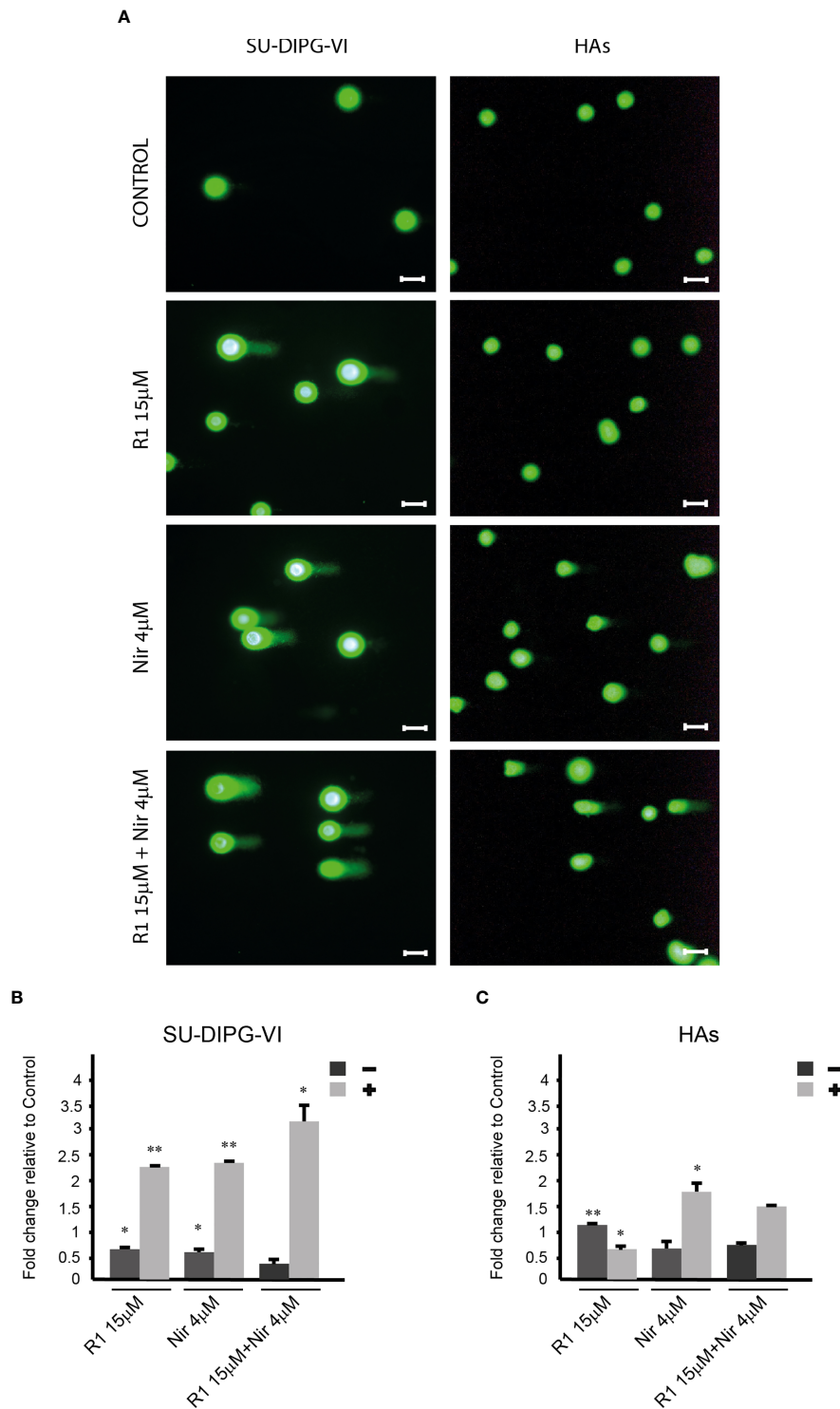


FIGURE 4
 The effect of raphin-1, niraparib, and their combination on DNA integrity. SU-DIPG-VI and HAS cells were plated and treated with raphin-1, niraparib, and their combination for 48 h, before performing the comet assay. (A). Images of SYBR Gold-stained cells. Bar, 100 μ m. (B, C). Treatment-induced changes in the fraction of cells with comets. Numbers are average \pm S.D of fold change relative to control from two or three independent experiments (HAS and SU-DIPG-VI, respectively). When indicated, p-values denote significance of differences among all experimental groups, as well as between each experimental group and control—* p < 0.05, ** p < 0.005. R1—Raphin-1, Nir—niraparib.

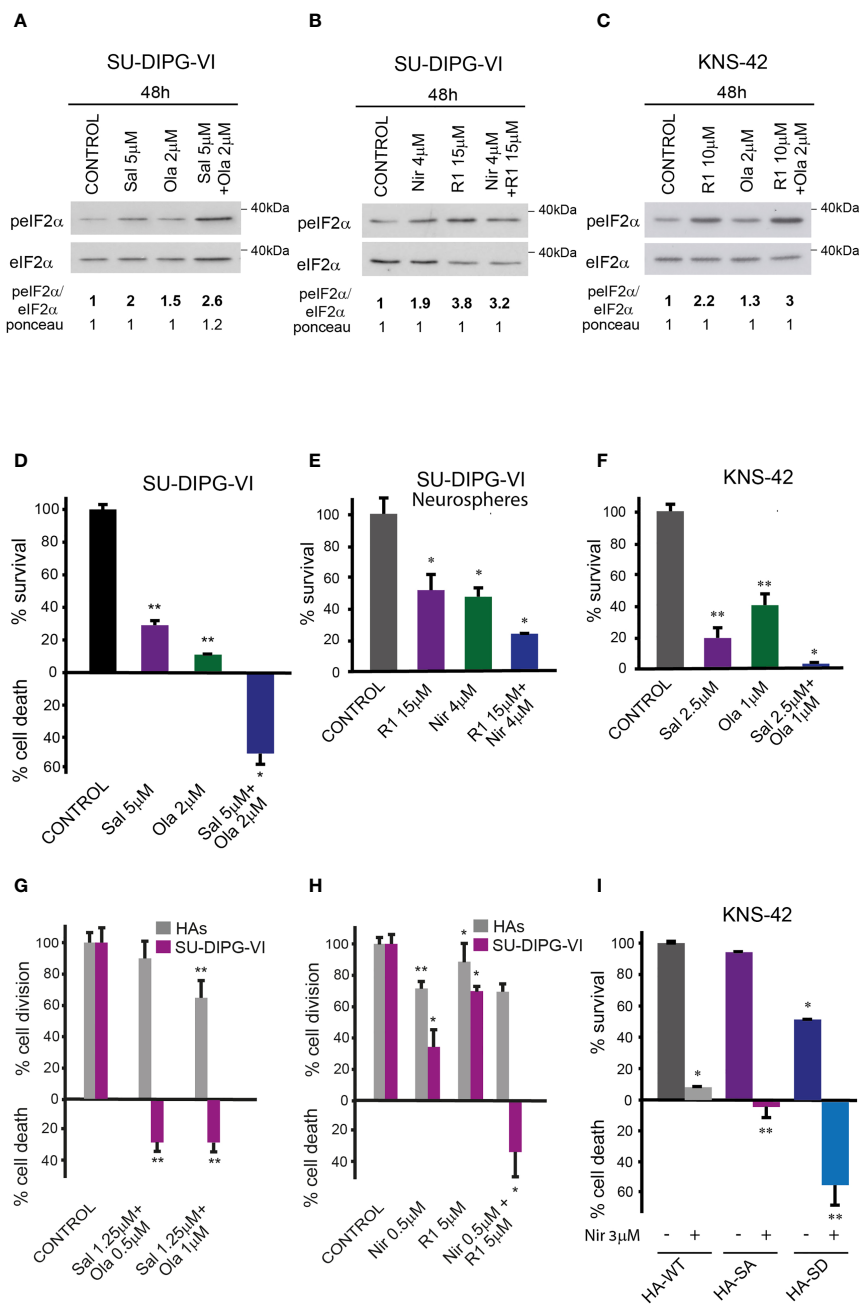


FIGURE 5

Combination of PARPis and salubrinal or raphin-1 enhanced the decrease in cell survival. (A–C) Cells were processed for Western blot analysis of treatment-induced changes in the ratio of pelf2α/eIF2α. Numbers at the bottom of the autoradiograms indicate changes of pelf2α/eIF2α and differences in loaded proteins (Ponceau) relative to control. (D, E). SU-DIPG-VI cells were plated at a density of 11,550 cells/cm², treated with drugs either 24 h (D) or 120 h (E) post-plating and incubated for additional 7 days. (F). KNS-42 cells were plated in triplicates for clonogenic assay at a density of 55 cells/cm² and treated with drugs 24 h post-plating. Values are mean survival or cell death (%) ± S.D relative to control. Differences among all experimental groups, as well as between each experimental group and control, were significant—*p < 0.05, **p < 0.005 (D–F). (G, H). SU-DIPG-VI and HAs cells were plated in triplicates at a density of 3,300 cells/cm² and treated with drugs 24 h post-plating. Values are mean number of cell division or cell death (%) ± S.D relative to control. Differences between treated and untreated experimental groups, as well as between SU-DIPG-VI and HAs, were significant—*p < 0.05, **p < 0.005. (I). KNS-42 cells were plated in duplicates at a density of 13,200 cells/cm² and transiently transfected with 1 μg/ml of plasmids expressing HA-eIF2α (HA-WT) or HA-S51A-eIF2α (HA-SA), or with HA-S51D-eIF2α (HA-SD) 24 h post-plating. Twenty-four hours later, cells were treated with niraparib for 6 days. Values are mean survival (%) ± S.D relative to control. Differences between survival of HA-SD with or without niraparib to either treated or untreated HA-SA or HA-WT were significant—*p < 0.05, **p < 0.005. Sal—salubrinal, R1—raphin-1, Ola—olaparib, Nir—niraparib. The experiments were reproduced at least twice with similar results.

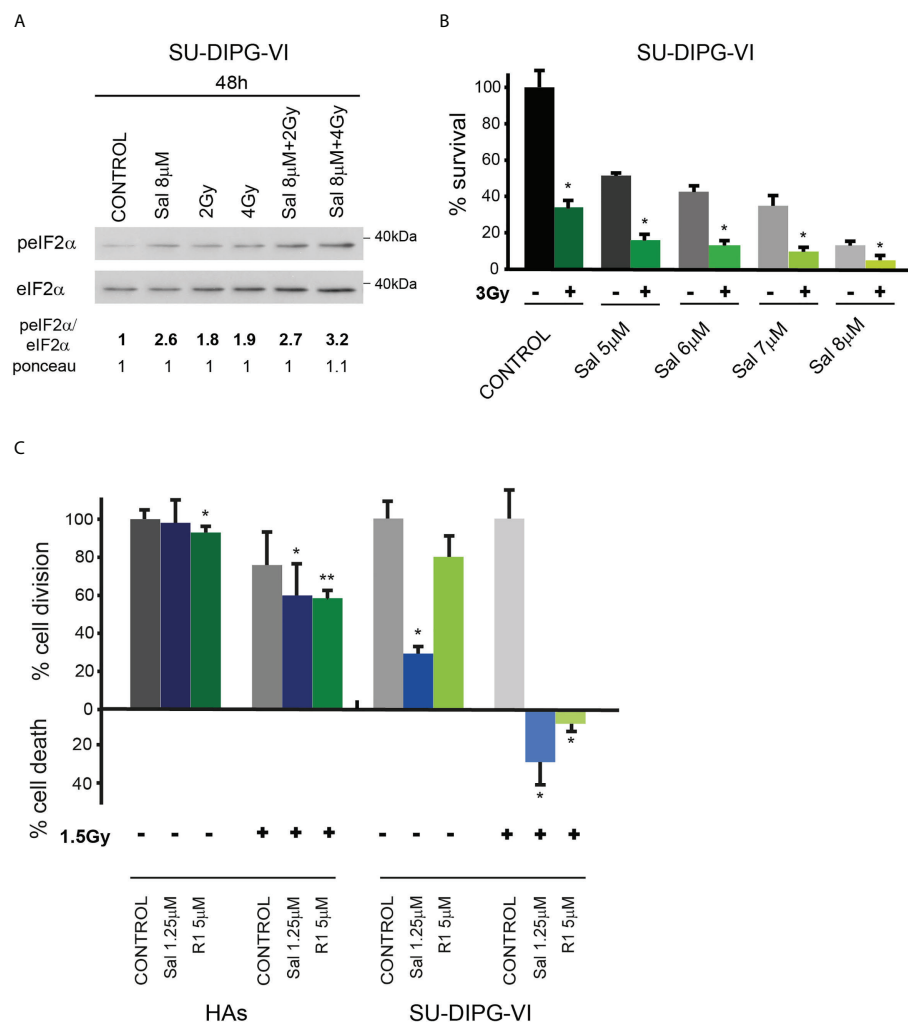


FIGURE 6

Combination of radiation with salubrinal or raphin-1 enhanced decrease in cell survival: (A). SU-DIPG-VI cells were irradiated and treated with drugs 24 h post-plating and incubated for additional 48 h before processing for Western blot analysis of treatment-induced changes in the ratio of p-eIF2 α /eIF2 α . Numbers at the bottom of the autoradiograms indicate changes of p-eIF2 α /eIF2 α and differences in loaded proteins (Ponceau) relative to control. (B). SU-DIPG-VI cells were plated in triplicates at a density of 11,500 cells/cm² and 24 h later were irradiated and treated with salubrinal. Cells were counted 7 days following treatment initiation. Values are mean survival (%) \pm S.D relative to control. Differences among all experimental groups, as well as between each experimental group and control, were significant—* p < 0.05. (C). SU-DIPG-VI and HA cells were plated in triplicates at a density of 3,300 cells/cm² and treated with drugs and radiation 24 h post-plating. Values are mean number of cell division or cell death (%) \pm S.D relative to control. Differences among all experimental groups as well as between each experimental group and control were significant for SU-DIPG-VI. When indicated, significance was observed between treated and control untreated HAs, but not among all experimental groups—* p < 0.05, ** p < 0.005. Gy—gray, Sal—salubrinal, R1—Raphin-1. The experiments were reproduced once with similar results.

eIF2Be level exceeded the minimal albeit reproducible effect of salubrinal. The observed difference may reflect a different interaction between the inhibitors and the holo-phosphatase complex and a role played by its components other than in modulating its enzymatic activity. Thus, the interaction of raphin-1 with the holo-phosphatase complex inhibits the recruitment of P-eIF2 α and leads to a p97 and proteasome-dependent degradation of CReP (32). In addition to the interaction of P-eIF2 α with the holo-phosphatase, it interacts

with CReP in complexes modulating intracellular traffic (43). Thus, a reduction in the level of CReP may increase the level of P-eIF2 α , which is free to interact with eIF2B. This interaction, in contrast to ISRIB, may destabilize the eIF2B complex (44), triggering the degradation of eIF2Be. Salubrinal and raphin-1 led to a similar increase of P-eIF2Be/eIF2Be, suggesting the decreased activity of the ERK-1/2 pathway, which is known to activate PP1 dephosphorylation and inhibition of GSK-3 β , thereby suppressing P-eIF2Be (19, 20).

By employing the comet assay, we demonstrated for the first time that an inhibitor of eIF2 α dephosphorylation affects DNA integrity. Relevant to this finding is our previous report that demonstrated the inhibitory effect of salubrinal on the repair of DNA double-strand breaks in green fluorescent protein reporter plasmids expressed in the breast cancer cell line (16), as well as the results of Choo et al. (45) regarding the inhibitory effect of increased P-eIF2 α on fork progression.

Exposing PED-GBM to the combination of PARPis with either salubrinal or raphin-1 decreased their survival relative to each drug alone. In addition, single SU-DIPG-VI cells and their neurospheres responded to the combination of raphin-1 and niraparib through an enhanced decrease in cell survival, suggesting that this combination may be effective *in vivo*. Under our experimental conditions, the level of P-eIF2 α in SU-DIPG-VI treated with the combination of raphin-1 and niraparib was higher than the level of P-eIF2 α in the niraparib-treated cells but was similar to that observed in the raphin-1-treated cells. This indicates that the treatment of PED-GBM with niraparib increases PED-GBM sensitivity to a further elevation of P-eIF2 α , while the treatment with raphin-1 increases PED-GBM sensitivity to a specific niraparib-induced damage that is yet to be defined. Finally, similar to raphin-1 and salubrinal, the S51D phosphomimetic eIF2 α variant increases the sensitivity of PED-GBM to niraparib, ascertaining the role of P-eIF2 α in modulating the PED-GBM response to PARPis.

As mentioned earlier, radiation is currently the sole treatment for DMG and results in only a few months of relief. Therefore, the effects of low concentrations of raphin-1 and salubrinal on the sensitivity of PED-GBM to low doses of ionizing radiation are of immediate clinical relevance. The effects of salubrinal and raphin-1 on the brain have been reported in several studies. In mouse models, increased P-eIF2 α by injecting salubrinal into the hippocampus impaired long-term memory (46). In addition, vanishing white matter syndrome is caused by the decreased activity of eIF2B (47), which can be affected by mutations or by increased P-eIF2 α . In contrast, in a mouse traumatic brain injury model, salubrinal suppressed endoplasmic reticulum (ER) stress, autophagy, and apoptosis (48). Moreover, administration of sephin1, an inhibitor of GADD34, was effective in two models of neurodegenerative diseases in mice that are associated with ER stress—Charcot-Marie-Tooth 1B (CMT-1B) and SOD1-ALS (49)—and administration of raphin-1 to mouse models of Huntington disease harboring the HD^{82Q} mutation improved their weight and decreased the SDS-insoluble huntingtin and nuclear assemblies in their cortices. Importantly, unlike salubrinal, raphin-1 did not have any adverse effect on the mice's memory (32). In addition, in contrast to its effect on PED-GBM, our experiments showed that raphin-1 decreased the fraction of cells with comet in HAs relative to the untreated control cells, and the sensitivity of HAs to raphin-1, salubrinal,

and their combination with either PARPis or ionizing radiation was remarkably lower than that of PED-GBM.

PED-GBM expressing either H3.1K27M or H3.3K27M define two subgroups of DMG. They differ in the distribution of the mutated histones in their chromatin leading to differences in gene expression and dependence on metabolic pathways (41, 42, 50, 51). Also, the two variants are associated with different additional mutations. While the H3.1K27M variant is associated with mutations in ACVR1 and PI3K pathway, the H3.3K27M variant is associated with mutations in the TP53 pathway (52, 53). However, alongside these differences there are similarities—and both H3.3K27M and H3.1K27M are dependent for their survival on the wnt/ β -catenin pathway (42). Defining the unique characteristics of each type of PED-GBM is extremely important for identifying molecular targets that will lead to the development of specific drugs for each type of PED-GBM, which may be more potent or specific relative to normal cells. At the moment, we do not know how and if the different H3 mutations (H3.1K27M, H3.3K27M, or H3.3G34R/V) or their associated mutations contribute to the sensitivity of PED-GBM to increased phosphorylation of eIF2 α . It is possible that the different GBM will be sensitive to the same drug either because they share a common dependence on a certain pathway or because these drugs may trigger different pathways in each one of them.

In summary, our studies point to drugs that modulate P-eIF2 α either alone or in combination with PARPis or ionizing radiation as novel means for treatment of PED-GBM and suggest that elucidation of their downstream effectors can reveal additional cellular components that can be targeted for the treatment of PED-GBM.

Data availability statement

The original contributions presented in the study are included in the article/[Supplementary Material](#). Further inquiries can be directed to the corresponding author.

Author contributions

KE, SP, MY, ZV, RO, JJ-H, GR, and AT designed the study and analyzed the data. KE, SP, and MY performed the experiments. KE, SP, MY, AT, and GR wrote the paper. ML and AH revised the manuscript. All authors contributed to the article and approved its submitted version.

Funding

This study was supported by funds from the Sheba Medical Center.

Acknowledgments

The authors thank Dr. Michelle Monje for the generous gift of the SU-DIPG cell lines. The work was performed in partial fulfillment of the requirements for the Ph.D. degree of Ziv Versano, Sackler School of Medicine, Tel-Aviv University. Some of the data appeared in preprint in the bioRxiv server (48).

Conflict of interest

The authors declare that the research was conducted in the absence of any commercial or financial relationships that could be construed as a potential conflict of interest.

References

- Khuong-Quang DA, Buczkowicz P, Rakopoulos P, Liu XY, Fontebasso AM, Bouffet E, et al. K27M mutation in histone H3.3 defines clinically and biologically distinct subgroups of pediatric diffuse intrinsic pontine gliomas. *Acta Neuropathol* (2012) 124(3):439–47. doi: 10.1007/s00401-012-0998-0
- Kallappagoudar S, Yadav RK, Lowe BR, Partridge JF. Histone H3 mutations—a special role for H3.3 in tumorigenesis? *Chromosoma* (2015) 124(2):177–89. doi: 10.1007/s00412-015-0510-4
- Harutyunyan AS, Krug B, Chen H, Papillon-Cavanagh S, Zeinieh M, De Jay N, et al. H3K27M induces defective chromatin spread of PRC2-mediated repressive H3K27me2/me3 and is essential for glioma tumorigenesis. *Nat Commun* (2019) 10(1):1262. doi: 10.1038/s41467-019-09140-x
- Haag D, Mack N, Benites Goncalves da Silva P, Statz B, Clark J, Tanabe K, et al. H3.3-K27M drives neural stem cell-specific gliomagenesis in a human iPSC-derived model. *Cancer Cell* (2021) 39(3):407–22 e13. doi: 10.1016/j.ccell.2021.01.005
- Jain SU, Rashoff AQ, Krabbenhoft SD, Hoelper D, Do TJ, Gibson TJ, et al. H3 K27M and EZHIP impede H3K27-methylation spreading by inhibiting allosterically stimulated PRC2. *Mol Cell* (2020) 80(4):726–35 e7. doi: 10.1016/j.molcel.2020.09.028
- Piunti A, Hashizume R, Morgan MA, Bartom ET, Horbinski CM, Marshall SA, et al. Therapeutic targeting of polycomb and BET bromodomain proteins in diffuse intrinsic pontine gliomas. *Nat Med* (2017) 23(4):493–500. doi: 10.1038/nm.4296
- Nagaraja S, Vitanza NA, Woo PJ, Taylor KR, Liu F, Zhang L, et al. Transcriptional dependencies in diffuse intrinsic pontine glioma. *Cancer Cell* (2017) 31(5):635–52 e6. doi: 10.1016/j.ccell.2017.03.011
- Huang TY, Piunti A, Qi J, Morgan M, Bartom E, Shilatfard A, et al. Effects of H3.3G34V mutation on genomic H3K36 and H3K27 methylation patterns in isogenic pediatric glioma cells. *Acta Neuropathol Commun* (2020) 8(1):219. doi: 10.1186/s40478-020-01092-4
- Cohen KJ, Pollack IF, Zhou T, Buxton A, Holmes EJ, Burger PC, et al. Temozolomide in the treatment of high-grade gliomas in children: a report from the children's oncology group. *Neuro Oncol* (2011) 13(3):317–23. doi: 10.1093/neuonc/nuq191
- Grasso CS, Tang Y, Truffaux N, Berlow NE, Liu L, Debily MA, et al. Functionally defined therapeutic targets in diffuse intrinsic pontine glioma. *Nat Med* (2015) 21(7):827. doi: 10.1038/nm.3855
- Chornenkyy Y, Agnihotri S, Yu M, Buczkowicz P, Rakopoulos P, Golbourn B, et al. Poly-ADP-Ribose polymerase as a therapeutic target in pediatric diffuse intrinsic pontine glioma and pediatric high-grade astrocytoma. *Mol Cancer Ther* (2015) 14(11):2560–8. doi: 10.1158/1535-7163.MCT-15-0282
- Yalon M, Tuval-Kochen L, Castel D, Moshe I, Mazal I, Cohen O, et al. Overcoming resistance of cancer cells to PARP-1 inhibitors with three different drug combinations. *PLoS One* (2016) 11(5):e0155711. doi: 10.1371/journal.pone.0155711
- Chao OS, Goodman OJr. Synergistic loss of prostate cancer cell viability by coinhibition of HDAC and PARP. *Mol Cancer Res* (2014) 12(12):1755–66. doi: 10.1158/1541-7786.MCR-14-0173

Publisher's note

All claims expressed in this article are solely those of the authors and do not necessarily represent those of their affiliated organizations, or those of the publisher, the editors and the reviewers. Any product that may be evaluated in this article, or claim that may be made by its manufacturer, is not guaranteed or endorsed by the publisher.

Supplementary material

The Supplementary Material for this article can be found online at: <https://www.frontiersin.org/articles/10.3389/fonc.2022.959133/full#supplementary-material>

- Gaymes TJ, Shall S, MacPherson LJ, Twine NA, Lea NC, Farzaneh F, et al. Inhibitors of poly ADP-ribose polymerase (PARP) induce apoptosis of myeloid leukemic cells: potential for therapy of myeloid leukemia and myelodysplastic syndromes. *Haematologica* (2009) 94(5):638–46. doi: 10.3324/haematol.2008.001933
- Konstantinopoulos PA, Wilson AJ, Saskowski J, Wass E, Khabele D. Suberoylanilide hydroxamic acid (SAHA) enhances olaparib activity by targeting homologous recombination DNA repair in ovarian cancer. *Gynecol Oncol* (2014) 133(3):599–606. doi: 10.1016/j.ygyno.2014.03.007
- Tuval-Kochen L, Paglin S, Keshet G, Lerenthal Y, Nakar C, Golani T, et al. Eukaryotic initiation factor 2alpha—a downstream effector of mammalian target of rapamycin—modulates DNA repair and cancer response to treatment. *PLoS One* (2013) 8(10):e77260. doi: 10.1371/journal.pone.0077260
- Versano Z, Shany E, Freedman S, Tuval-Kochen L, Leitner M, Paglin S, et al. MutT homolog 1 counteracts the effect of anti-neoplastic treatments in adult and pediatric glioblastoma cells. *Oncotarget* (2018) 9(44):27547–63. doi: 10.18632/oncotarget.25547
- Wek RC. Role of eIF2alpha kinases in translational control and adaptation to cellular stress. *Cold Spring Harb Perspect Biol* (2018) 10(7). doi: 10.1101/cshperspect.a032870
- Cagnetta R, Wong HH, Frese CK, Mallucci GR, Krijgsvelde J, Holt CE. Noncanonical modulation of the eIF2 pathway controls an increase in local translation during neural wiring. *Mol Cell* (2019) 73(3):474–89 e5. doi: 10.1016/j.molcel.2018.11.013
- Quevedo C, Salinas M, Alcazar A. Initiation factor 2B activity is regulated by protein phosphatase 1, which is activated by the mitogen-activated protein kinase-dependent pathway in insulin-like growth factor 1-stimulated neuronal cells. *J Biol Chem* (2003) 278(19):16579–86. doi: 10.1074/jbc.M212936200
- Baird TD, Wek RC. Eukaryotic initiation factor 2 phosphorylation and translational control in metabolism. *Adv Nutr* (2012) 3(3):307–21. doi: 10.3945/an.112.002113
- Nova I, Zeng H, Harding HP, Ron D. Feedback inhibition of the unfolded protein response by GADD34-mediated dephosphorylation of eIF2alpha. *J Cell Biol* (2001) 153(5):1011–22. doi: 10.1083/jcb.153.5.1011
- Harding HP, Zhang Y, Scheuner D, Chen JJ, Kaufman RJ, Ron D. Ppp1r15 gene knockout reveals an essential role for translation initiation factor 2 alpha (eIF2alpha) dephosphorylation in mammalian development. *Proc Natl Acad Sci U.S.A.* (2009) 106(6):1832–7. doi: 10.1073/pnas.0809632106
- Tian X, Zhang S, Zhou L, Seyhan AA, Hernandez Borrero L, Zhang Y, et al. Targeting the integrated stress response in cancer therapy. *Front Pharmacol* (2021) 12:747837. doi: 10.3389/fphar.2021.747837
- Jousse C, Oyadomari S, Nova I, Lu P, Zhang Y, Harding HP, et al. Inhibition of a constitutive translation initiation factor 2alpha phosphatase, CREP, promotes survival of stressed cells. *J Cell Biol* (2003) 163(4):767–75. doi: 10.1083/jcb.200308075
- Chen R, Rato C, Yan Y, Crespiello-Casado A, Clarke HJ, Harding HP, et al. G-Actin provides substrate-specificity to eukaryotic initiation factor 2alpha holophosphatases. *Elife* (2015) 4. doi: 10.7554/eLife.04871

27. Chambers JE, Dalton LE, Clarke HJ, Malzer E, Dominicus CS, Patel V, et al. Actin dynamics tune the integrated stress response by regulating eukaryotic initiation factor 2 α dephosphorylation. *Elife* (2015) 4. doi: 10.7554/eLife.04872
28. Boyce M, Bryant KF, Jousse C, Long K, Harding HP, Scheuner D, et al. A selective inhibitor of eIF2 α dephosphorylation protects cells from ER stress. *Science* (2005) 307(5711):935–9. doi: 10.1126/science.1101902
29. Cnop M, Ladriere L, Hekerman P, Ortis F, Cardozo AK, Dogusan Z, et al. Selective inhibition of eukaryotic translation initiation factor 2 α phosphorylation potentiates fatty acid-induced endoplasmic reticulum stress and causes pancreatic beta-cell dysfunction and apoptosis. *J Biol Chem* (2007) 282(6):3989–97. doi: 10.1074/jbc.M607627200
30. Scheuner D, Song B, McEwen E, Liu C, Laybutt R, Gillespie P, et al. Translational control is required for the unfolded protein response and *in vivo* glucose homeostasis. *Mol Cell* (2001) 7(6):1165–76. doi: 10.1016/S1097-2765(01)00265-9
31. Crespillo-Casado A, Chambers JE, Fischer PM, Marciniak SJ, Ron D. PPP1R15A-mediated dephosphorylation of eIF2 α is unaffected by Sepsin1 or guanabenz. *Elife* (2017) 6. doi: 10.7554/eLife.26109
32. Krzyzosiak A, Sigurdardottir A, Luh L, Carrara M, Das I, Schneider K, et al. Target-based discovery of an inhibitor of the regulatory phosphatase PPP1R15B. *Cell* (2018) 174(5):1216–28 e19. doi: 10.1016/j.cell.2018.06.030
33. Schoof M, Boone M, Wang L, Lawrence R, Frost A, Walter P. eIF2B conformation and assembly state regulate the integrated stress response. *Elife* (2021) 10. doi: 10.7554/eLife.65703.sa2
34. Peidis P, Papadakis AI, Muaddi H, Richard S, Koromilas AE. Doxorubicin bypasses the cytoprotective effects of eIF2 α phosphorylation and promotes PKR-mediated cell death. *Cell Death Differ* (2011) 18(1):145–54. doi: 10.1038/cdd.2010.76
35. Persaud L, Zhong X, Alvarado G, Do W, Dejoie J, Zytseva A, et al. eIF2 α phosphorylation mediates IL24-induced apoptosis through inhibition of translation. *Mol Cancer Res* (2017) 15(8):1117–24. doi: 10.1158/1541-7786.MCR-16-0454
36. Chi AS, Tarapore RS, Hall MD, Shonka N, Gardner S, Umemura Y, et al. Pediatric and adult H3 K27M-mutant diffuse midline glioma treated with the selective DRD2 antagonist ONC201. *J Neurooncol* (2019) 145(1):97–105. doi: 10.1007/s11060-019-03271-3
37. Kline CL, Van den Heuvel AP, Allen JE, Prabhu VV, Dicker DT, El-Deiry WS. ONC201 kills solid tumor cells by triggering an integrated stress response dependent on ATF4 activation by specific eIF2 α kinases. *Sci Signal* (2016) 9(415):ra18. doi: 10.1126/scisignal.aac4374
38. Paglin S, Lee NY, Nakar C, Fitzgerald M, Plotkin J, Deuel B, et al. Rapamycin-sensitive pathway regulates mitochondrial membrane potential, autophagy, and survival in irradiated MCF-7 cells. *Cancer Res* (2005) 65(23):11061–70. doi: 10.1158/0008-5472.CAN-05-1083
39. Chou TC. Drug combination studies and their synergy quantification using the chou-talalay method. *Cancer Res* (2010) 70(2):440–6. doi: 10.1158/0008-5472.CAN-09-1947
40. Min A, Im SA. PARP inhibitors as therapeutics: Beyond modulation of PARylation. *Cancers (Basel)* (2020) 12(2):394. doi: 10.3390/cancers12020394
41. Castel D, Philippe C, Calmon R, Le Dret L, Truffaux N, Boddaert N, et al. Histone H3F3A and HIST1H3B K27M mutations define two subgroups of diffuse intrinsic pontine gliomas with different prognosis and phenotypes. *Acta Neuropathol* (2015) 130(6):815–27. doi: 10.1007/s00401-015-1478-0
42. Nagaraja S, Quezada MA, Gillespie SM, Arzt M, Lennon JJ, Woo PJ, et al. Histone variant and cell context determine H3K27M reprogramming of the enhancer landscape and oncogenic state. *Mol Cell* (2019) 76(6):965–80 e12. doi: 10.1016/j.molcel.2019.08.030
43. Kloft N, Neukirch C, von Hoven G, Bobkiewicz W, Weis S, Boller K, et al. A subunit of eukaryotic translation initiation factor 2 α -phosphatase (CreP/PPP1R15B) regulates membrane traffic. *J Biol Chem* (2012) 287(42):35299–317. doi: 10.1074/jbc.M112.379883
44. Bogorad AM, Lin KY, Marintchev A. Novel mechanisms of eIF2B action and regulation by eIF2 α phosphorylation. *Nucleic Acids Res* (2017) 45(20):11962–79. doi: 10.1093/nar/gkx845
45. Choo J, Schlosser D, Manzini V, Magerhans A, Dobbstein M. The integrated stress response induces r-loops and hinders replication fork progression. *Cell Death Dis* (2020) 11(7):538. doi: 10.1038/s41419-020-2727-2
46. Costa-Mattioli M, Gobert D, Stern E, Gamache K, Colina R, Cuello C, et al. eIF2 α phosphorylation bidirectionally regulates the switch from short- to long-term synaptic plasticity and memory. *Cell* (2007) 129(1):195–206. doi: 10.1016/j.cell.2007.01.050
47. Wong YL, LeBon L, Basso AM, Kohlhaas KL, Nikkel AL, Robb HM, et al. eIF2B activator prevents neurological defects caused by a chronic integrated stress response. *Elife* (2019) 8. doi: 10.7554/eLife.42940
48. Wang ZF, Gao C, Chen W, Gao Y, Wang HC, Meng Y, et al. Salubrinal offers neuroprotection through suppressing endoplasmic reticulum stress, autophagy and apoptosis in a mouse traumatic brain injury model. *Neurobiol Learn Mem* (2019) 161:12–25. doi: 10.1016/j.nlm.2019.03.002
49. Das I, Krzyzosiak A, Schneider K, Wrabetz L, D'Antonio M, Barry N, et al. Preventing proteostasis diseases by selective inhibition of a phosphatase regulatory subunit. *Science* (2015) 348(6231):239–42. doi: 10.1126/science.aaa4484
50. Sarthy JF, Meers MP, Janssens DH, Henikoff JG, Feldman H, Paddison PJ, et al. Histone deposition pathways determine the chromatin landscapes of H3.1 and H3.3 K27M oncohistones. *Elife* (2020) 9. doi: 10.7554/eLife.61090
51. Sturm D, Witt H, Hovestadt V, Khuong-Quang DA, Jones DT, Konermann C, et al. Hotspot mutations in H3F3A and IDH1 define distinct epigenetic and biological subgroups of glioblastoma. *Cancer Cell* (2012) 22(4):425–37. doi: 10.1016/j.ccr.2012.08.024
52. Buczkowicz P, Hoeman C, Rakopoulos P, Pajovic S, Letourneau L, Dzamba M, et al. Genomic analysis of diffuse intrinsic pontine gliomas identifies three molecular subgroups and recurrent activating ACVR1 mutations. *Nat Genet* (2014) 46(5):451–6. doi: 10.1038/ng.2936
53. Fontebasso AM, Papillon-Cavanagh S, Schwartzentruber J, Nikbakht H, Gerges N, Fiset PO, et al. Recurrent somatic mutations in ACVR1 in pediatric midline high-grade astrocytoma. *Nat Genet* (2014) 46(5):462–6. doi: 10.1038/ng.2950